

# Motion-Zero: Zero-Shot Moving Object Control Framework for Diffusion-Based Video Generation

Changgu Chen, Junwei Shu, Lianggangxu Chen, Gaoqi He,  
Changbo Wang\* and Yang Li\*

School of Science and Technology, East China Normal University  
52215901006@stu.ecnu.edu.cn, {cbwang,yli}@cs.ecnu.edu.cn

## Abstract

Recent large-scale pre-trained diffusion models have demonstrated a powerful generative ability to produce high-quality videos from detailed text descriptions. However, exerting control over the motion of objects in videos generated by any video diffusion model is a challenging problem. In this paper, we propose a novel zero-shot moving object trajectory control framework, Motion-Zero, to enable a bounding-box-trajectories-controlled text-to-video diffusion model. To this end, an initial noise prior module is designed to provide a position-based prior to improve the stability of the appearance of the moving object and the accuracy of position. In addition, based on the attention map of the U-net, spatial constraints are directly applied to the denoising process of diffusion models, which further ensures the positional and spatial consistency of moving objects during the inference. Furthermore, temporal consistency is guaranteed with a proposed shift temporal attention mechanism. Our method can be flexibly applied to various state-of-the-art video diffusion models without any training process. Extensive experiments demonstrate our proposed method can control the motion trajectories of objects and generate high-quality videos.

## 1 Introduction

In recent years, the generative capabilities of diffusion models have been widely recognized in both text-to-image [Dhariwal and Nichol, 2021; Ho *et al.*, 2020; Rombach *et al.*, 2022; Song *et al.*, 2020] and text-to-video domains [Guo *et al.*, 2023; Ho *et al.*, 2022]. Although these video models are capable of producing high-definition, high-resolution, and fluid video animations, the dynamic motion trajectories of the generated objects are relatively random in existing text-to-video models [Blattmann *et al.*, 2023; Zhang *et al.*, 2023a]. Thus, accurate control of an object’s motion trajectories in a generated video remains rudimentary.

To address this problem, various efforts have been proposed in different strategies. Some methods [Zhang *et al.*,

2023b; Wu *et al.*, 2023a] try to control the trajectory of the moving object by providing a detailed conditional motion sequence, such as a dancing skeleton. However, the cost of acquiring conditional control sequences is non-negligible and inhibits the diverse generation of video outputs by the user. To obtain variety over the generated video with more control capability, i.e. trajectories of moving objects, several methods [Wang *et al.*, 2023c; Wang *et al.*, 2023b; Yin *et al.*, 2023] harness a substantial dataset of motion and trajectory pairs to train the baseline models. Although the results are very impressive and promising, these methods are solely applicable to the base models on which they were trained and cannot be applied to other models directly. Furthermore, all of these methods require extensive training and significant computational resources, preventing ordinary users from using them.

Nevertheless, the fundamental text-to-video diffusion models [Blattmann *et al.*, 2023; Zhang *et al.*, 2023a] have undergone an extremely large scale training dataset [Bain *et al.*, 2021; Xue *et al.*, 2022]. Theoretically, the pre-trained model should inherently have learned extensive knowledge about the dynamics of a variety of object movements. However, the semantics of the latent space in different modules of a video diffusion model are not explicitly defined, which makes it difficult to manually control generated video in desired motion dynamics. To some extent, methods mentioned above try to align and define those latent spaces in the baseline model by training with additional labeled datasets, and successfully harness the intrinsic knowledge of pre-trained models to control the motion. In addition, we observe that the initial noise plays a significant inspirational role in the generation of the videos. The same initial noise tends to produce videos with similar content. With these two characteristics, we can manipulate the trajectory of moving objects.

In this paper, we propose a zero-shot framework, Motion-Zero, that can be easily applied to any pre-trained video diffusion model and achieve universality and plug-and-play capabilities of controlling. To this end, we designed an initial noise prior module to provide noises based on the motion trajectories given by the user. Inspired by the fact that the values of the cross-attention map within the U-Net largely determine the generation location of the subject mentioned in the prompt [Xie *et al.*, 2023; Epstein *et al.*, 2023], spatial constraints with an attention similarity loss over these attention

\*corresponding authors

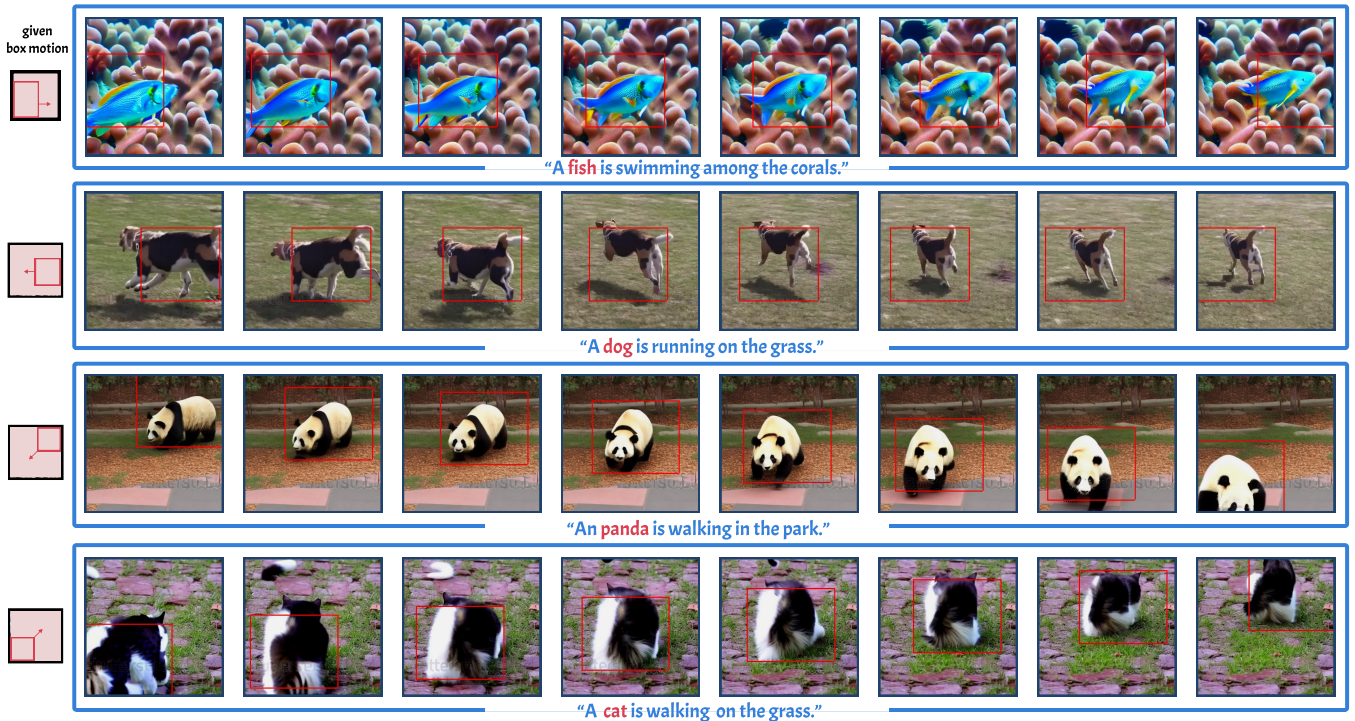


Figure 1: Our Motion-Zero framework endows any pre-trained video diffusion model with the capability to manipulate object trajectories directly, circumventing the need for supplementary training. By designating the target entity in the input prompts and a sequence of bounding boxes, users can intuitively direct the motion path of the object within the generated video sequence.

maps are proposed to achieve precise manipulation of object positioning within individual frames. Furthermore, based on our observations, we find that merely imposing spatial constraints on the positions of objects can negatively impact the overall coherence and video quality. To preserve the continuity throughout the video sequence, a novel shift temporal attention mechanism is proposed to further maintain the baseline model focus on the same objects across the time axis. Through the implementation of these modules, our framework can effectively generate high-quality video controlled by bounding-box trajectories without any training process. Samples generated by Motion-Zero can be viewed in Fig. 1. The main innovations of our work can be summarized as follows,

- We propose a zero-shot framework Motion-Zero which is capable of controlling the motion trajectories of arbitrary objects within a pre-trained video generation diffusion model. Our Motion-Zero is plug-and-play and without any additional training.
- By recognizing the influence of initial noise on video generation, we implemented an initial noise conditioning module that establishes advantageous starting conditions for controllable video diffusion.
- To further accurate control over the generative video, we propose spatial constraints and a novel shift temporal attention mechanism aimed at ensuring the positional accuracy and temporal continuity and consistency of the target, respectively.

- Extensive experiments demonstrate that our proposed work can be applied to any pre-trained video diffusion models. Our results can outperform those from extensively pre-trained trajectory control models.

## 2 Related Works

### 2.1 Text-To-Video Diffusion Models

As text-to-image diffusion models have flourished and demonstrated impressive results, the body of work related to text-to-video diffusion has gradually expanded. Researchers and developers are leveraging the principles of text-to-image models to extend their capabilities into the dynamic and temporally complex domain of video generation. In the realm of text-to-video (T2V) synthesis, the field has witnessed several pioneering approaches. Initial endeavors such as Imagen Video [Ho *et al.*, 2022] and Make-A-Video [Singer *et al.*, 2022] tackled T2V generation at the pixel level, leading to notable advancements but also encountering constraints in video duration and quality due to computational intensity. To address these limitations, MagicVideo [Zhou *et al.*, 2022] emerged, introducing a novel autoencoder trained specifically on video data, which, akin to the impact of Latent Diffusion Models (LDMs) [Rombach *et al.*, 2022] in the text-to-image (T2I) sector, significantly improved the computational efficiency of T2V tasks. In the current landscape, there exists an abundance of generalizable open-domain text-to-video generation models capable of producing high-definition videos with dynamic visual fidelity [Blattmann *et al.*, 2023;

Zhang *et al.*, 2023a; Mullan *et al.*, 2023; Sterling, 2023; Chen *et al.*, 2023; Wang *et al.*, 2023a]. The models often generate either stochastic motion paths or demonstrate relatively minor variations in dynamics, underscoring the potential benefits of investigating methodologies for manually stipulating more deliberate and varied motion trajectories.

## 2.2 Controllable Video Generalization

There are now pre-trained methodologies [Wang *et al.*, 2023c; Wang *et al.*, 2023b; Yin *et al.*, 2023] in place that have the capability to control the motion trajectories of objects within generated videos. VideoComposer [Wang *et al.*, 2023b] employs a two-stage training strategy to incrementally incorporate temporal information and control signals. A motion condition encoder is proposed for training, designed to enhance the model’s ability to understand and integrate motion-specific information. DragNUMA [Yin *et al.*, 2023] also employs a comparable training strategy and utilizes optical flow as a conditioning mechanism for trajectory modeling. MotionCtrl [Wang *et al.*, 2023c] synthesizes the approaches of these two works and introduces a camera control module and a trajectory control module to further refine the management of movement within generated video content. These models typically rely on extensive training on large-scale datasets such as WebVid-10M [Bain *et al.*, 2021] and HD-VILA-100M [Xue *et al.*, 2022] which lead to expensive training costs. Also, these models are typically constrained to operate on the specific models they were trained on, lacking the flexibility to interchange base video diffusion models. This limitation hinders their adaptability and limits the scope of their application to only those scenarios for which they were explicitly designed. Our model stands out in that it can be applied to any base diffusion model without the necessity for further training. This versatility not only broadens its applicability but also results in substantial savings in training costs and resources, offering a significant advantage over more rigid, model-specific methods. A contemporaneous work [Ma *et al.*, 2023] parallels our approach with a similar zero-shot setting. However, they ignore the importance of the initial noise and the control of spatial and temporal consistency.

## 3 Preliminaries

**Video Diffusion Model:** Video diffusion models are designed to produce high-quality and diverse videos, guided by text prompts. To save the computational costs, [Rombach *et al.*, 2022] utilize a U-Net as a denoising model within a latent space, significantly reducing the computational load in terms of both time and space.

In detail, these models employ a Variational Autoencoder (VAE), which comprises an encoder  $\mathcal{E}$  and a decoder  $\mathcal{D}$ . The encoder compresses the original video from pixel space into a latent representation, and the decoder reconstructs the video from this latent space back to pixel space. The 3D U-Net typically consists of a series of down-sampling blocks, middle blocks, and up-sampling blocks. Each block is equipped with convolutional layers, spatial transformers, and temporal transformers. The optimization of the 3D U-Net (denoted as

$\epsilon_\theta$ ) is executed through a noise prediction loss function:

$$\mathcal{L} = \mathcal{E}_{\mathbf{z}_0, \mathbf{c}, \epsilon \sim \mathcal{N}(0, \mathbf{I}), t} [\|\epsilon - \epsilon_\theta(\mathbf{z}_t, t, \mathbf{c})\|_2^2], \quad (1)$$

where  $\mathbf{z}_0$  is the latent code of the training videos,  $\mathbf{c}$  is the text prompt condition,  $\epsilon$  is the Gaussian noise added to the latent code, and  $t$  is the time step. The noised latent code  $\mathbf{z}_t$  is determined as:

$$\mathbf{z}_t = \sqrt{\bar{a}_t} \mathbf{z}_0 + \sqrt{1 - \bar{a}_t} \epsilon, \bar{a}_t = \prod_{i=1}^t a_i, \quad (2)$$

where  $a_t$  is a hyper-parameter used for controlling the noise strength based on time  $t$ .

**Motion Trajectory Control:** Based on video diffusion, the task of motion trajectory control is to precisely control the motion trajectory of objects in generated videos. The optimization objective can be formulated as:

$$\mathcal{L} = \mathcal{E}_{\mathbf{z}_0, \mathbf{c}, \epsilon \sim \mathcal{N}(0, \mathbf{I}), t} [\|\epsilon - \epsilon_\theta(\mathbf{z}_t, t, \mathbf{c}, \mathcal{B})\|_2^2]. \quad (3)$$

Specifically, users can input a text condition  $\mathbf{c}$  along with a sequence of rectangular boxes  $\mathcal{B} = \{(x_1^f, y_1^f), (x_2^f, y_2^f)\}^{N_f}$ , where  $(x_1^f, y_1^f), (x_2^f, y_2^f)$  are the upper left and lower right points of the box in frame  $f$ ,  $N_f$  is the total frame number. The boxes  $\mathcal{B}$  correspond to an the position of the moving object.

## 4 Methodology

### 4.1 Overview

Existing trajectory control methods require large-scale video training data to optimize Eq.3 leading to a high computational cost. Differently, our work falls into the setting of zero-shot motion trajectory control. To this end, our Motion-Zero framework operates entirely during the inference stage, thus eliminating the need for any training and making it compatible with any pre-trained video diffusion model.

In the following section, we provide a detailed presentation of the proposed Motion-Zero framework and its individual components. The pipeline is shown in Fig.2 (a). Sec.4.2 introduces the designed initial noise prior module. Sec.4.3 is followed to describe how we constrain the moving object position and spatial consistency. Finally, Sec.4.4 details our shift temporal attention mechanism which improves the temporal consistency.

### 4.2 Initial Noise Prior Module

According to the theory of DDIM Inversion [Ho *et al.*, 2020], the initial noise has a significant impact on the final generated outcome. The Initial Noise Prior Module (INPM) is designed to leverage this property to provide a strong prior for the position of the moving object. Several steps are involved to integrate a moving object into a sequence of frames with a coherent prior as shown in Fig.2 (b). Firstly, a meta video  $V_{meta}$  is sampled using the original Video Diffusion with spatial constraints (introduced in Sec.4.3),  $\mathbf{z}^* \sim \mathcal{N}(0, \mathbf{I})$  as latent input, conditioned on a given prompt  $\mathbf{c}$  and the first frame box  $\mathcal{B}^0$ . Then, a video latent  $\mathbf{z}_{meta}$  is generated based on  $V_{meta}$  from Encoder  $\mathcal{E}$ . Once  $\mathbf{z}_{meta}$  is prepared, we perform a DDIM

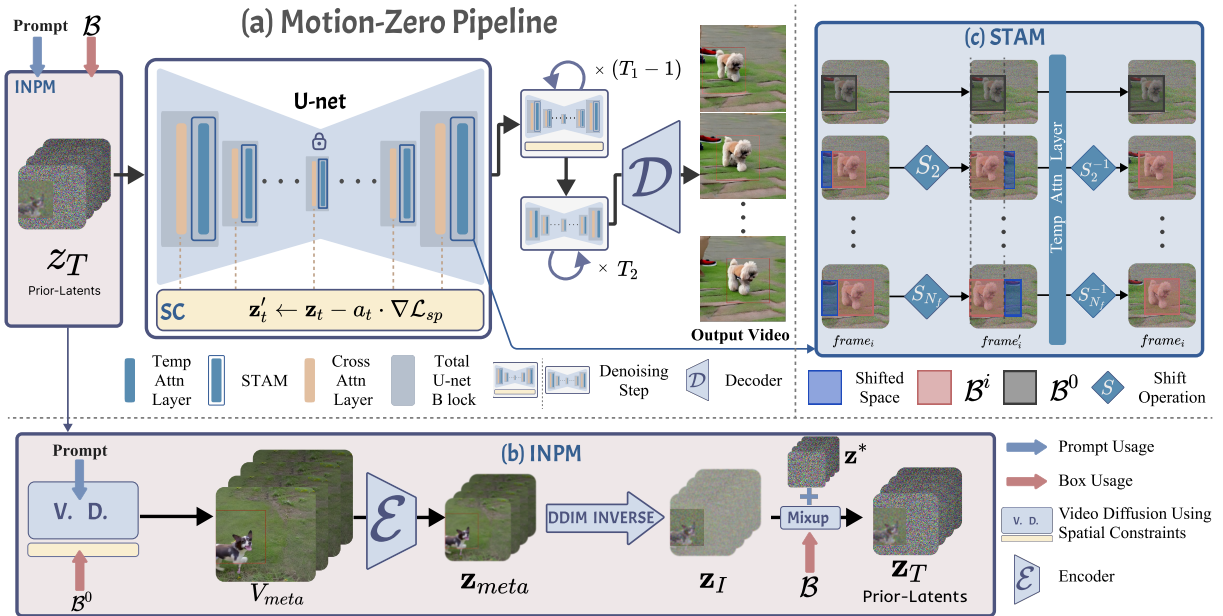


Figure 2: Overview of our Motion-Zero. The total pipeline is shown on (a). Given the box condition  $\mathcal{B}$  and the prompt condition, we generate the prior latents  $\mathbf{z}_T$  by our Initial Noise Prior Module (INPM) as shown on (b). At timestep  $t$ ,  $\mathbf{z}_t$  is firstly optimized to  $\mathbf{z}'_t$  by the Spatial Constraints (SC). Subsequently,  $\mathbf{z}'_t$  is passed to the U-net with Shift Temporal Attention Module (STAM) as demonstrated on (c). All the parameters of the video diffusion are frozen.  $T_1$  represents the number of timesteps during which SC and STAM are applied, and  $T_2$  denotes the number of timesteps where the original video diffusion process is utilized.

### Algorithm 1 Initial Noise Prior Module

**Input:**  $\mathbf{c}, \mathcal{B}$

**Parameter:**  $N_f, \lambda_p$

**Function:**  $\text{Pixel}(\mathbf{a}, \mathbf{b})$  means the elements get from tensor  $\mathbf{a}$  in the range of box  $\mathbf{b}$

**Output:** Initial noise  $\mathbf{z}^*$

- 1:  $\mathbf{z}^* \sim \mathcal{N}(0, \mathbf{I})$   $\triangleright$  random sample the first latent code
- 2:  $\mathbf{V}_{meta} \leftarrow \text{VideoDiffusion}(\mathbf{z}^*, \mathbf{c}, \mathcal{B}_0)$   $\triangleright$  Video Diffusion using SC, the first box and  $\mathbf{c}$  as condition
- 3:  $\mathbf{z}_{meta} \leftarrow \text{Encoder}(\mathbf{V}_{meta})$
- 4:  $\mathbf{z}_I \leftarrow \text{DDIM\_Inverse}(\mathbf{z}_{meta})$   $\triangleright$  inverse the  $\mathbf{z}_{meta}$
- 5:  $\mathbf{z}_T \leftarrow \mathbf{z}^*$
- 6: **for** all  $f=1,2,\dots,N_f$  **do**
- 7:  $\text{Pixel}(\mathbf{z}_T^f, \mathcal{B}^f) \leftarrow \lambda_p \cdot \text{Pixel}(\mathbf{z}_I^f, \mathcal{B}^0) + (1 - \lambda_p) \cdot \text{Pixel}(\mathbf{z}_T^f, \mathcal{B}^f)$   $\triangleright$  local mixup operation
- 8: **end for**
- 9: **return**  $\mathbf{z}_T$   $\triangleright$  initial latent with position prior

Inversion to obtain the corresponding noise latent representation  $\mathbf{z}_I$ . We crop the latent representation within the box  $\mathcal{B}^0$  for each frame, creating a sequence of latent patches. Subsequently, we use a local mixup operation [Zhang *et al.*, 2017] to mix the latent patches and the initial noise  $\mathbf{z}^*$  in the range of  $\mathcal{B}^f$  frame by frame. This method allows us to set a coherent prior in the corresponding object’s position in the initial noises. It also ensures that the animated object maintains consistency in appearance and movement across the video frames, without incurring additional computational costs during the generation process. Details are shown in Alg.1.

### 4.3 Spatial Constraints with Attention Map

The INPM alone is insufficient for precise manipulation of an object’s trajectory. To further improve the capability of control, we introduce Spatial Constraints (SC) deployed at each denoising step  $t$  to optimize the intermediate latent representation  $\mathbf{z}_t$ . This optimization is crucial for enhancing the accuracy of the moving object position and preserving spatial consistency. Within the conditional denoising architecture, cross-attention serves as the pivotal bridge that connects the text prompt with the content generated. During the denoising steps, conditioned on the prompt  $\mathbf{c}$  and the intermediate features  $\mathbf{z}_t$ , the corresponding cross-attention map can be obtained as  $\mathbf{A}$ :

$$\mathbf{A} = \text{Softmax}(\mathbf{Q}\mathbf{K}^\top / \sqrt{d}), \quad (4)$$

$$\mathbf{Q} = \mathbf{W}_Q \mathbf{z}_t, \mathbf{K} = \mathbf{W}_K \mathbf{c}, \quad (5)$$

where  $\mathbf{Q}, \mathbf{K}$  are the query and key of the  $\mathbf{z}_t$  and  $\mathbf{c}$ , respectively.  $\mathbf{W}_Q, \mathbf{W}_K$  are two learnable matrices, which are frozen in our settings. Assuming a maximum number  $N_p$  of prompt tokens  $\{\mathbf{p}_1, \dots, \mathbf{p}_{N_p}\}$  in condition  $\mathbf{c}$ , at time step  $t$ , it is feasible to derive  $N_p$  cross-attention maps  $\{\mathbf{A}_1, \dots, \mathbf{A}_{N_p}\}$ .

When a user specifies the index  $k$  of prompt tokens  $\mathbf{p}_k$  intended to control the trajectory of an object, along with the box  $\mathcal{B}$ , the box-loss can be employed to ensure that our model controls the object to appear within the input box in every frame. Specifically, the box-loss is achieved through an optimization approach that maximizes the values of the  $\mathbf{A}_k$  for the corresponding prompt tokens inside the box, while minimizing the values outside the box. Frame by frame, we scale down the user-specified coordinate box to the corresponding coordinates in the latent space and construct a mask  $\mathbf{M}^f$

where 1 for areas in the box and 0 otherwise. To ensure the values inside the box for attention are maximized, we propose an intuitive solution  $\mathcal{L}_i$  as

$$\mathcal{L}_i^f = 1 - \frac{1}{P} \sum \mathbf{g}(\mathbf{A}_k^f \cdot \mathbf{M}^f, P), \quad (6)$$

where  $\mathbf{g}(\cdot, P)$  means the top  $P$  highest value will be selected. If we employ all the values within the attention maps, it could disrupt the stability of the denoising process. Conversely, utilizing too few values could result in a less pronounced control effect. On the other hand, we aim for the attention values outside the box to be as minimal as possible which is formulated as

$$\mathcal{L}_o^f = \frac{1}{P} \sum \mathbf{g}(\mathbf{A}_k^f \cdot (1 - \mathbf{M}^f), P). \quad (7)$$

Within these two constraints, we can ensure that the object generated in each frame is contained within the box. However, there is no guarantee that the object will be positioned at the center of the box. To mitigate this, we propose another center-loss  $\mathcal{L}_c$  to encourage the centroid of the  $\mathbf{A}_k^f$  to closely align with the center of the box as

$$[W_{\mathbf{A}_k^f}, H_{\mathbf{A}_k^f}] = \frac{1}{\sum_{w,h} \mathbf{A}_{k,w,h}^f} [\sum_{w,h} w \cdot \mathbf{A}_{k,w,h}^f, \sum_{w,h} h \cdot \mathbf{A}_{k,w,h}^f], \quad (8)$$

$$\mathcal{L}_c^f = \left\| \left( \frac{x_1^f + x_2^f}{2}, \frac{y_1^f + y_2^f}{2} \right) - (W_{\mathbf{A}_k^f}, H_{\mathbf{A}_k^f}) \right\|_1, \quad (9)$$

where  $\mathbf{A}_{k,w,h}^f$  is the value of  $\mathbf{A}_k^f$  at the position of  $(w, h)$ ,  $(W_{\mathbf{A}_k^f}, H_{\mathbf{A}_k^f})$  is the centroid position of  $\mathbf{A}_k^f$ . After establishing robust control over the position of the object, we recognize unexpected variations in the object’s appearance due to the substantial extent of movement. To ensure appearance consistency across frames, we strive to maintain the uniformity of the  $\mathbf{A}_k^f$  within the box. To this end, we introduce a similarity loss  $\mathcal{L}_s$  as

$$\mathcal{L}_s = 1 - \frac{1}{N_f - 1} \sum_f^{\text{Pixel}(\mathbf{A}_i^f, \mathcal{B}^f), \text{Pixel}(\mathbf{A}_i^{f+1}, \mathcal{B}^{f+1})} \text{Sim}(\text{Pixel}(\mathbf{A}_i^f, \mathcal{B}^f), \text{Pixel}(\mathbf{A}_i^{f+1}, \mathcal{B}^{f+1})), \quad (10)$$

where  $\text{Sim}(\cdot, \cdot)$  means the similarity of two elements and  $\text{Pixel}(\cdot)$  is a function getting corresponding elements of the map  $\mathbf{A}^f$  within a box range  $\mathcal{B}^f$ . Cosine similarity is adopted here. At each timestep, the overall spatial constraints  $\mathcal{L}_{sp}$  are formulated as follows:

$$\mathcal{L}_{sp} = \sum_f (\lambda_i \mathcal{L}_i^f + \lambda_o \mathcal{L}_o^f + \lambda_c \mathcal{L}_c^f) + \lambda_s \mathcal{L}_s, \quad (11)$$

where  $\lambda_i, \lambda_o, \lambda_c, \lambda_s$  are hyper-parameters. By minimizing and calculating the gradient of the Eq.11, we can optimize our latent  $\mathbf{z}_t$  in Eq.2 as follows: S

$$\mathbf{z}'_t \leftarrow \mathbf{z}_t - \beta_t \cdot \nabla \mathcal{L}_{sp}, \quad (12)$$

where  $\beta_t$  linearly decays at each timestep  $t$ . Specifically, before denoising with the U-Net at each timestep  $t$ , we update  $\mathbf{z}_t$  to  $\mathbf{z}'_t$  using Eq.12. Then, we continue the denoising process using  $\mathbf{z}'_t$ . Under the combined effect of the aforementioned constraints, the latent variable  $\mathbf{z}_t$  at each timestep will

gradually shift towards generating high-response attention in the specified position, while ensuring that the appearance attributes of the object within the box remain unchanged. Consequently, the target object is synthesized within the bounding box area provided by the user.

#### 4.4 Shift Temporal Attention Mechanism

After the spatial constraints on attention maps, pre-trained video diffusion models still encounter difficulties in generating sequences of continuous actions. Within the temporal module of the diffusion process, the latent representation is reshaped into the following configuration (using einops [Rogozhnikov, 2021] notation):

$$\text{rearrange}(\mathbf{z}, \text{b f c h w} \rightarrow (\text{b h w}) \text{f c}),$$

where  $\text{b}$  means batch size,  $\text{f}$  represents frame number,  $\text{c}$  is the channel number and  $\text{w}, \text{h}$  means the width and the height. Within the temporal transformer, attention is focused on the same pixel across different frames. This leads to a scenario where, if the extent of motion is too large, the same position in different frames could undergo significant semantic changes, resulting in a lack of coherence in the generated dynamics.

To overcome this inconsistency, we propose a Shift Temporal Attention Mechanism (STAM) to improve the dynamics of the moving object in different frames. Specifically, we shift the elements of  $\mathbf{z}^f$  inside the  $\mathcal{B}^f$  range with the elements inside the  $\mathcal{B}^0$  range, as shown in Fig.2 (b). Therefore, the subsequent frames within the box range can be aligned with the box range of the first frame. The steps are shown as follows,

$$\begin{aligned} \mathbf{z}_w^f &= \text{Shift}(\mathbf{z}^f, \mathcal{B}^f, \mathcal{B}^0), \\ \mathbf{z}_w' &= \text{TemporalAttention}(\mathbf{z}_w), \\ \mathbf{z}^{f'} &= \text{Shift}(\mathbf{z}_w', \mathcal{B}^0, \mathcal{B}^f), \end{aligned} \quad (13)$$

where  $\text{Shift}(\cdot, a, b)$  is the shift operation,  $\mathbf{z}_w^f$  means the shifted latent  $\mathbf{z}^f$  of frame  $f$  and  $\mathbf{z}_w = [\mathbf{z}_w^1, \dots, \mathbf{z}_w^f]$ . By applying STAM to a **TemporalAttention** layer, we can achieve coherence in the motion of moving objects without additional training, and without incurring extra computational costs during inference.

## 5 Experiments

### 5.1 Implementation Details

Our algorithm is fully implemented during the inference stage, thus it does not require any training. The hyper-parameter  $\lambda_i, \lambda_o$  are set to 1,  $\lambda_c$  is set to 0.05,  $\lambda_s$  is set to 0.5,  $\lambda_p$  is set to 0.8. To balance the trade-off between the size of GPU memory consumption and the semantic information retained in the attention map  $\mathbf{A}$ , we chose a  $48 \times 48$  size for  $\mathbf{A}$  when the output resolution is  $384 \times 384$ . We use DDIM [Song *et al.*, 2020] as our sampling method. In the experiment,  $T_1$  in Fig.2 is set as 10, which means the SC and the STAM are employed during the first 10 timesteps;  $T_2$  is set to 20, thus the total denoising timestep  $T$  is 30. All of our experiments are conducted on a single A100 GPU.



Figure 3: Quality comparison results on different methods. We take one frame from every three frames. The input prompt of left part: *A fish is swimming in the sea.* Right part: *A bear is walking on the grass.* We employed ModelScope (a) and ZeroScope (b) as our baseline models and compared the effect of incorporating additional prompts with the integration of our Motion-Zero. In addition, we conducted a comparative analysis with the pre-trained MotionCtrl model (c). The red dots serve as the control conditions. **Zoom in for the best view.**

## 5.2 Comparisons with Others

We evaluate the effectiveness of our method from both qualitative and quantitative perspectives. Two video diffusion baseline methods [Sterling, 2023; Wang *et al.*, 2023a] are involved to confirm that our approach maintains generative performance. In addition, the SOTA pre-trained model MotionCtrl [Wang *et al.*, 2023c] is also involved in experiments to demonstrate the control ability of our proposed method.

**Qualitative Results.** The results of the qualitative experiments are shown in Fig.3. The base model depicted in the first two rows of the figure is ModelScope. The first row incorporates additional input boxes and utilizes the Motion-Zero framework, while in the second row, an extra prompt is added: *moving from left to right.* As shown in the first row left, the fish follows a trajectory that strictly adheres to the positions of the boxes. Conversely, in the second row left, the direction of the fish’s movement is not fixed, and the locations where it appears are generated randomly. In the second row right, the bear gradually rotates clockwise and fails to follow the guidance provided by the additional prompts. We can see that the model controlled by the Motion-Zero framework is capable of more effectively governing the trajectory and direction of an object’s movement which cannot be achieved by prompts alone. The base model for the third and fourth rows is ZeroScope. In the third row, both the fish and the bear move according to the conditions set by our boxes, whereas in the fourth row, they remain mostly stationary. This shows that our Motion-Zero model effectively facilitates trajectory control across various baseline models. The fifth row in the figure demonstrates the effects of the pre-trained model MotionCtrl. It can be seen that our results are comparable to those of the pre-trained model in terms of controlling the direction of the movements of the fish. In the case of generating a bear,

MotionCtrl only manages to rotate the bear’s body, whereas Motion-Zero can effectively generate the bear’s movement. Note that our method additionally allows for the control of their size. Our advantage also lies in the ability to plug and play with any base model without the need for any training.

**Quantitative Results with Automatic Metrics.** Followed by LOVEU-TGVE competition [Wu *et al.*, 2023b], the CLIP score [Hessel *et al.*, 2021] is used to verify text-video consistency (Text Align) and inter-frame consistency (Consistency). The PickScore [Kirstain *et al.*, 2023] is used to predict user preferences of our model. We utilized five prompts, with each prompt generating ten videos to serve as test data. The results are shown in Tab.1. From the first four rows of the table, we can discern that employing our Motion-Zero framework to direct the motion trajectory of objects does not compromise the base model’s performance. Instead, the motion subject being constrained by the box results in improved semantic accuracy and temporal consistency. Upon examining the fifth row of the table, it is evident that Motion-Zero achieves an enhancement in performance over pre-trained methodology.

**User Study.** We recruited 5 voters from social media to evaluate 10 generated videos from the aspect of appearance, temporal consistency, and control capacity, which evaluate whether the position of the moving object is similar to the references. Voters are presented with pairs of videos in a randomized sequence without revealing the creation methods. They are then tasked with assessing each pair and indicating which video they find more favorable. The results are shown in Tab.2. The number in the table denotes the number of Motion-Zero enhanced videos preferred by the voters. v.s. ZeroScope and v.s. ModelScope are the two baseline methods supplemented with guiding prompts, for instance, *moving from left to right.* v.s. MotionCtrl is a comparison between

	Text Align	Consistency	PickScore
ZeroScope	20.05	0.89	18.15
+Ours	22.04	<b>0.93</b>	<b>20.00</b>
ModelScope	20.30	0.91	18.56
+Ours	<b>24.74</b>	0.91	19.82
MotionCtrl	20.94	0.92	19.62

Table 1: Automatic metric on baseline methods and SOTA methods. All metrics are such that higher values indicate better performance.

	Appearance	Consistency	Control
v.s. ZeroScope	41/50	20/50	46/50
v.s. ModelScope	38/50	34/50	46/50
v.s. MotionCtrl	25/50	23/50	36/50

Table 2: User study on different motion control methods.

ZeroScope augmented with our Motion-Zero and the standalone MotionCtrl approach with the same control trajectory. We can see that the voters prefer our methods from all aspects compared with baselines. Moreover, when compared to MotionCtrl, users demonstrated a clear preference for the control capabilities of Motion-Zero. Note that our proposed approach does not need any training. Thus, the baseline model’s inherent limitations resulted in our approach being slightly inferior to MotionCtrl in aspects of consistency.

### 5.3 Ablation Study

We conduct a series of ablation experiments to verify the effectiveness of our modules individually.

**Impact of INPM.** INPM is designed to provide a prior for the initial position of moving objects, facilitating the model to more stably control the position of the object’s movement. As shown in Fig.4, the second row demonstrates the effects of removing this module. We can see that the lion is not entirely within the frame, and due to the forceful control by SC, the lion’s body undergoes significant deformation, while the lion’s head shows no movement at all. For Motion-Zero, the lion’s body is clearly generated, and the lion’s head also moves with the changes in the frame, resulting in the high overall stability of the lion. This shows that the INPM module plays a significant role in stably controlling the position of objects and generating stable videos.

**Impact of SC.** In this section, we validate the importance of SC. SC primarily provides auxiliary support for control over spatial positioning. As shown in the third line in Fig.4, without spatial constraints, the generated motion of the lion appears mostly outside the box. The SC is the most important module for our Motion-Zero controlling method. The reason is that SC is the only gradient-based modification to the baseline compared with other modules.

**Impact of STAM.** The role of the STAM is to ensure the temporal consistency of the moving object, which is to maintain the continuity of its motion as it moves. As illustrated in Fig.4, we present the effects of omitting the STAM module in the last row. It can be noted that during the movement, the lion’s legs undergo deformation and become blurred. In



Figure 4: Ablation studies on different components. We use ZeroScope as our baseline model. To demonstrate the coherence of the generated object’s motion, we captured every other frame, resulting in a total of 6 frames. The prompt is *A lion is walking on the field.* **Zoom in for the best view.**

contrast, the first row demonstrates that the lion’s leg movements are well-generated with strong continuity, highlighting the significance of our STAM. More details are provided in the supplementary materials.

## 6 Discussion, Limitation and Future Works

Due to the absence of the need for additional training, our method can be applied to all pre-trained video diffusion models. However, on the other hand, its generative performance is entirely dependent on the base model. Existing video diffusion models sometimes generate relatively unstable objects, such as deformation in moving objects, holes in the background, and various issues like the inability to precisely control the attributes of generated objects with text.

Our method can currently effectively control the movement of objects in videos, but the trajectory of the movement is entirely controlled by the user, lacking semantic interaction with the video. For example, in a forest scene, if a user provides the first frame as a reference, they can use a prompt like *a little rabbit goes to the stream to drink water* to control a rabbit to navigate and avoid obstacles in the forest automatically. This kind of interaction between object movement and the background, as well as narrative-like semantic control, will be the direction of our future work.

## 7 Conclusion

In this paper, we proposed a framework Motion-Zero for controlling object motion that can be applied to any video diffusion model. Unlike previous methods that require extensive training, our method enables arbitrary motion control in a zero-shot setting. We find that the initial noise plays a significant role in object motion, leading us to introduce an initial noise prior module to achieve stable control effects. We discovered that the values in the cross-attention map significantly influence the position and appearance of the object corresponding to the prompt. Therefore, spatial constraints are designed to optimize the position of moving objects and

ensure spatial consistency. Furthermore, to ensure the consistency of object motion, a shift temporal attention mechanism is developed to maintain the temporal coherence of moving objects. Extensive experiments substantiate the efficacy and generalization of our approach.

## References

- [Bain *et al.*, 2021] Max Bain, Arsha Nagrani, Gül Varol, and Andrew Zisserman. Frozen in time: A joint video and image encoder for end-to-end retrieval. In *IEEE International Conference on Computer Vision*, 2021.
- [Blattmann *et al.*, 2023] Andreas Blattmann, Tim Dockhorn, Sumith Kulal, Daniel Mendeleevitch, Maciej Kilian, Dominik Lorenz, Yam Levi, Zion English, Vikram Voleti, Adam Letts, et al. Stable video diffusion: Scaling latent video diffusion models to large datasets. *arXiv preprint arXiv:2311.15127*, 2023.
- [Chen *et al.*, 2023] Haoxin Chen, Menghan Xia, Yingqing He, Yong Zhang, Xiaodong Cun, Shaoshu Yang, Jinbo Xing, Yaofang Liu, Qifeng Chen, Xintao Wang, Chao Weng, and Ying Shan. Videocrafter1: Open diffusion models for high-quality video generation, 2023.
- [Dhariwal and Nichol, 2021] Prafulla Dhariwal and Alexander Nichol. Diffusion models beat gans on image synthesis. *Advances in neural information processing systems*, 34:8780–8794, 2021.
- [Epstein *et al.*, 2023] Dave Epstein, Allan Jabri, Ben Poole, Alexei A Efros, and Aleksander Holynski. Diffusion self-guidance for controllable image generation. *arXiv preprint arXiv:2306.00986*, 2023.
- [Guo *et al.*, 2023] Yuwei Guo, Ceyuan Yang, Anyi Rao, Yaohui Wang, Yu Qiao, Dahua Lin, and Bo Dai. AnimateDiff: Animate your personalized text-to-image diffusion models without specific tuning. *arXiv preprint arXiv:2307.04725*, 2023.
- [Hessel *et al.*, 2021] Jack Hessel, Ari Holtzman, Maxwell Forbes, Ronan Le Bras, and Yejin Choi. Clipscore: A reference-free evaluation metric for image captioning. *arXiv preprint arXiv:2104.08718*, 2021.
- [Ho *et al.*, 2020] Jonathan Ho, Ajay Jain, and Pieter Abbeel. Denoising diffusion probabilistic models. *Advances in neural information processing systems*, 33:6840–6851, 2020.
- [Ho *et al.*, 2022] Jonathan Ho, William Chan, Chitwan Saharia, Jay Whang, Ruiqi Gao, Alexey Gritsenko, Diederik P Kingma, Ben Poole, Mohammad Norouzi, David J Fleet, et al. Imagen video: High definition video generation with diffusion models. *arXiv preprint arXiv:2210.02303*, 2022.
- [Kirstain *et al.*, 2023] Yuval Kirstain, Adam Polyak, Uriel Singer, Shahbuland Matiana, Joe Penna, and Omer Levy. Pick-a-pic: An open dataset of user preferences for text-to-image generation. *arXiv preprint arXiv:2305.01569*, 2023.
- [Ma *et al.*, 2023] Wan-Duo Kurt Ma, J. P. Lewis, and W. Kleijn. Trailblazer: Trajectory control for diffusion-based video generation. 2023.
- [Mullan *et al.*, 2023] John Mullan, Duncan Crawbuck, and Aakash Sastry. Hotshot-XL, October 2023.
- [Rogozhnikov, 2021] Alex Rogozhnikov. Einops: Clear and reliable tensor manipulations with einstein-like notation. In *International Conference on Learning Representations*, 2021.
- [Rombach *et al.*, 2022] Robin Rombach, Andreas Blattmann, Dominik Lorenz, Patrick Esser, and Björn Ommer. High-resolution image synthesis with latent diffusion models. In *Proceedings of the IEEE/CVF conference on computer vision and pattern recognition*, pages 10684–10695, 2022.
- [Singer *et al.*, 2022] Uriel Singer, Adam Polyak, Thomas Hayes, Xi Yin, Jie An, Songyang Zhang, Qiyuan Hu, Harry Yang, Oron Ashual, Oran Gafni, et al. Make-a-video: Text-to-video generation without text-video data. *arXiv preprint arXiv:2209.14792*, 2022.
- [Song *et al.*, 2020] Jiaming Song, Chenlin Meng, and Stefano Ermon. Denoising diffusion implicit models. *arXiv preprint arXiv:2010.02502*, 2020.
- [Sterling, 2023] Spencer Sterling. ZeroScope, October 2023.
- [Wang *et al.*, 2023a] Jiuniu Wang, Hangjie Yuan, Dayou Chen, Yingya Zhang, Xiang Wang, and Shiwei Zhang. Modelscope text-to-video technical report. *arXiv preprint arXiv:2308.06571*, 2023.
- [Wang *et al.*, 2023b] Xiang Wang, Hangjie Yuan, Shiwei Zhang, Dayou Chen, Jiuniu Wang, Yingya Zhang, Yujun Shen, Deli Zhao, and Jingren Zhou. Videocomposer: Compositional video synthesis with motion controllability. *arXiv preprint arXiv:2306.02018*, 2023.
- [Wang *et al.*, 2023c] Zhouxia Wang, Ziyang Yuan, Xintao Wang, Tianshui Chen, Menghan Xia, Ping Luo, and Ying Shan. Motionctrl: A unified and flexible motion controller for video generation. *arXiv preprint arXiv:2312.03641*, 2023.
- [Wu *et al.*, 2023a] Jay Zhangjie Wu, Yixiao Ge, Xintao Wang, Stan Weixian Lei, Yuchao Gu, Yufei Shi, Wynne Hsu, Ying Shan, Xiaohu Qie, and Mike Zheng Shou. Tune-a-video: One-shot tuning of image diffusion models for text-to-video generation. In *Proceedings of the IEEE/CVF International Conference on Computer Vision*, pages 7623–7633, 2023.
- [Wu *et al.*, 2023b] Jay Zhangjie Wu, Xiuyu Li, Difei Gao, Zhen Dong, Jinbin Bai, Aishani Singh, Xiaoyu Xiang, Youzeng Li, Zuwei Huang, Yuanxi Sun, Rui He, Feng Hu, Junhua Hu, Hai Huang, Hanyu Zhu, Xu Cheng, Jie Tang, Mike Zheng Shou, Kurt Keutzer, and Forrest Iandola. Cvpr 2023 text guided video editing competition, 2023.
- [Xie *et al.*, 2023] Jinheng Xie, Yuexiang Li, Yawen Huang, Haozhe Liu, Wentian Zhang, Yefeng Zheng, and Mike Zheng Shou. Boxdiff: Text-to-image synthesis with training-free box-constrained diffusion. In *Proceedings of the IEEE/CVF International Conference on Computer Vision*, pages 7452–7461, 2023.

- [Xue *et al.*, 2022] Hongwei Xue, Tiankai Hang, Yanhong Zeng, Yuchong Sun, Bei Liu, Huan Yang, Jianlong Fu, and Baining Guo. Advancing high-resolution video-language representation with large-scale video transcriptions. In *Proceedings of the IEEE/CVF Conference on Computer Vision and Pattern Recognition*, pages 5036–5045, 2022.
- [Yin *et al.*, 2023] Shengming Yin, Chenfei Wu, Jian Liang, Jie Shi, Houqiang Li, Gong Ming, and Nan Duan. Drag-nuwa: Fine-grained control in video generation by integrating text, image, and trajectory. *arXiv preprint arXiv:2308.08089*, 2023.
- [Zhang *et al.*, 2017] Hongyi Zhang, Moustapha Cisse, Yann N Dauphin, and David Lopez-Paz. mixup: Beyond empirical risk minimization. *arXiv preprint arXiv:1710.09412*, 2017.
- [Zhang *et al.*, 2023a] David Junhao Zhang, Jay Zhangjie Wu, Jia-Wei Liu, Rui Zhao, Lingmin Ran, Yuchao Gu, Difei Gao, and Mike Zheng Shou. Show-1: Marrying pixel and latent diffusion models for text-to-video generation. *arXiv preprint arXiv:2309.15818*, 2023.
- [Zhang *et al.*, 2023b] Lvmin Zhang, Anyi Rao, and Maneesh Agrawala. Adding conditional control to text-to-image diffusion models. *ArXiv*, abs/2302.05543, 2023.
- [Zhou *et al.*, 2022] Daquan Zhou, Weimin Wang, Hanshu Yan, Weiwei Lv, Yizhe Zhu, and Jiashi Feng. Magicvideo: Efficient video generation with latent diffusion models. *arXiv preprint arXiv:2211.11018*, 2022.